Journal of Inorganic and Organometallic Polymers and Materials (2021) 31:3867–3879
https://doi.org/10.1007/s10904-021-01992-5

Facile Modification of Biochar Derived from Agricultural Straw Waste with Effective Adsorption and Removal of Phosphorus from Domestic Sewage

Junjie Yuan[1] · Yao Zhu[2] · Jizhang Wang[1] · Zhigang Liu[3] · Meiying He[2] · Tao Zhang[2] · Pingping Li[1] · Fengxian Qiu[2]

Received: 27 February 2021 / Accepted: 29 March 2021 / Published online: 7 April 2021

Abstract
In recent decades, straw waste is the major byproduct around agriculture that has become one of the factors of environmental pollution. The purpose of this study is to reuse waste straw to develop a new green and highly efficient biomass-based adsorbent for phosphorus removal. To attain this aim, Mg–Al bimetallic oxide/straw fiber (Mg–Al/SF) with hierarchical structure was successfully synthesized by hydrothermal method using waste straw as the biomass carbon precursor and Mg–Al/SF was applied as adsorbent in the removal of phosphorus from wastewater. The morphology, composition and structure of the adsorbent was well supported by several characterizations. The prepared biomass-based adsorbent showed outstanding adsorption performance. Maximum adsorption capability of Mg–Al/SF towards phosphorus from the Langmuir isotherm model was fitted out to be 89.37 mg/g. The related kinetics and isotherm study for the adsorption process were explored in detail. The proposed adsorbent exhibited good reusability that the removal of phosphorus remained above 72% after 5 cycles. In addition, thermodynamic study was carried out to further investigate the phosphorus removal mechanism, which was the synergistic combination of surface adsorption and chemical adsorption. The removal of total phosphorus in actual domestic sewage (Total phosphorus, TP, 0.8–1.1 mg/L) were investigated. The results indicated that the prepared Mg–Al/SF has excellent TP adsorption and recycling performance, and the adsorption and stability performance are significantly higher than that of the commercial activated carbon. The interactions between biomass material with large surface area and metal oxide provides great potential for the real application in the water treatment. Furthermore, it also presents a feasible and efficient practical example of increasing the use of agricultural waste.

Keywords Biomass · Agricultural waste · Wastewater treatment · Synergistic adsorption · Phosphorus removal

1 Introduction

With the increasing development of sustainable agriculture on a global scale, comprehensive utilization of agricultural wastes and effective improvement of natural environment have become great concern over the decades. The worldwide agricultural wastes are partially served as recyclable resources utilized in the daily life such as high-quality fertilizer providers, however, these wastes have been one of the representatives for environment pollutants in most areas. To reduce the pollution caused by agricultural wastes and enhance the application of natural wastes, it's of great interest in the reutilization of renewable sources from the environment to prepare functional materials. Numerous reports have investigated the availability of different agricultural wastes and their applications, including corncob, coffee shell, mushroom waste and other byproducts [1–3]. Against

Junjie Yuan and Yao Zhu contributed equally to this work and should be considered co-first authors.

✉ Pingping Li
lipingping@ujs.edu.cn

✉ Fengxian Qiu
fxqiu@ujs.edu.cn

[1] School of Agricultural Engineering, Jiangsu University, Zhenjiang 212013, China

[2] School of Chemistry and Chemical Engineering, Jiangsu University, Zhenjiang 212013, China

[3] School of Environment and Safety Engineering, Jiangsu University, Zhenjiang 212013, China

the background, using waste agriculture products to exploit green, efficient and sustainable advanced material has been a focus in the current research.

Recently, biomass materials converted from natural waste have received great attention as renewable and sustainable sources due to the advantage of easy availability, low cost and environmentally friendly feature [4, 5]. Biomass is an inexhaustible source of carbon as its precursor is extensively distributed in the environment, which exhibits great potential in the application of adsorption [6], catalysis [7], energy storage [8] and drug delivery [9]. The access to the resource of biomass-based materials is extensive [10]. Up to now, biomass carbon materials can be obtained by thermal approaches including conventional pyrolysis, microwave pyrolysis and hydrothermal methods. The familiar abandoned straw can be taken as an excellent agricultural waste source to be fabricated into biomass carbon material with high specific area and prominent pore structure, which is a feasible adsorbent for wastewater treatment with great development potential [11–13]. However, the pristine biomass carbon fiber with few kinds of functional groups on the surface cannot meet the demand in the practical adsorption process. To achieve superior adsorption property based on biomass carbon material, various modification strategies have been employed to decorate the fiber surface via a simple and effective way, of which constructing metal oxide on the biomass carbon substrate is recognized as a useful method that can enhance the adsorption performance via synergistic effect.

In recent decades, eutrophication of water body caused by phosphorus pollution has seriously endangered human life and environmental safety [14, 15]. Although phosphorus is of vital importance to the environment, it's urgent to reduce the phosphorus content in the water via modern technologies. Numerous reports on dephosphorization from wastewater have summarized the common method, however, seeking an efficient, eco-friendly and low-cost method is still on the search [16]. Physical method for phosphorus removal is expensive and inefficient, and the emerging biological method is highly dependent on the environment with poor practicability. Traditional chemical method has only a little effect on the low concentration of phosphorus in the real wastewater, which requires a mass of chemical agents and may cause secondary contamination [17–19]. In contrast, adsorption has attracted much attention in the field of phosphorus removal that opens the possibility of phosphorus desorption from materials and phosphorus recovery from wastewater [20–22]. Notably, phosphorus removal research is being carried out worldwide, involving synthesizing adsorbent materials from waste to reduce production costs and create more environmentally friendly materials [17, 23]. Hence, it is reasonable that using agricultural straw waste-derived biomass material as suitable adsorbent for efficient removal of phosphorus with the concept of green chemical development.

In this work, straw waste was used as carbon precursors to prepare magnesium aluminum bimetallic oxide modified biomass-based composite with hierarchical structure by hydrothermal method, which was applied as regenerated environmental remediation adsorbent for phosphorus removal. Magnesium and aluminum composite oxide were constructed on straw fiber via in situ growth method. Based on the synergistic effect among straw fiber, magnesium ion and aluminum ion in the composite material, the adsorption property was enhanced, and the stability and electronic conductivity were also improved. The detailed adsorption process was investigated, and possible adsorption mechanism was also raised. The adsorbent has a broad application prospect in enhancing the adsorption capacity of phosphorus and other pollutants in wastewater.

2 Experimental Section

2.1 Raw Material

Abandoned straw fiber were collected from the surrounding farm. Sodium hydroxide (NaOH), hydrochloric acid (HCl), sodium chlorite, hexamethylenetetramine ($C_6H_{12}N_4$), aluminium nitrate nonahydrate ($Al(NO_3)_3{\cdot}9H_2O$), acetic acid (HAc), magnesium nitrate hexahydrate ($Mg(NO_3)_2{\cdot}6H_2O$), Potassium dihydrogen phosphate (KH_2PO_4) were purchased from Sinopharm Chemical Reagent Co. Ltd. (China). All the reagents used were of analytical grade. The deionized water was prepared by the laboratory system.

2.2 Preparation of Mg–Al Multiple Oxide/Biomass Composite (Mg–Al/SF)

10 g of dried rice straw was cut into pieces and immersed in 1 M sodium hydroxide solution (300 mL). Then the rice straw was stirred under 80 °C to remove impurities. After reacting for 3 h, the straw fibers were washed with deionized water until the filtrate becomes transparent. The fibers were dispersed in 100 mL of 5% acidified sodium chlorite solution at 80 °C for decolorization. After 3 h, the biomass fibers were collected and washed with deionized water until the pH of filtrate reached neutral. The obtained straw fiber (SF) was dried in an oven overnight for further use.

The preparation of Mg–Al/SF was as follow. At first, 150 mg of SF was immersed in 200 mL deionized water containing 10 g of $Al(NO_3)_3{\cdot}9H_2O$ for 8 h, then the dried fibers heated at 400 °C under nitrogen atmosphere for 4 h continuously to obtain Al_2O_3/SF. Mg–Al/SF was fabricated by hydrothermal reaction. 1.2045 g of $Mg(NO_3)_2{\cdot}6H_2O$, 0.49 g of the above Al_2O_3/SF and 0.674 g

of hexamethylenetetramine (HMT) were well dispersed in 75 mL of deionized water. The mixture was transferred to an autoclave heating at 120 °C for 12 h. After filtration, the products were washed and dried in an oven at 50 °C for 3 h. Finally, the dried fibers were heated to 500 °C under the protection of nitrogen for 4 h to obtain Mg–Al multiple oxide/biomass composite (Mg–Al/SF) material. The synthetic process of Mg–Al/SF is shown in Scheme 1.

2.3 Adsorption Experiment

To test the adsorption performance of Mg–Al/SF towards phosphorus from aqueous solution, 25 mg of Mg–Al/SF was dispersed in 10 mL of KH_2PO_4 solution (100 mg/L). The adsorption process was carried out at room temperature for 2 h. After reaching equilibrium, the sample was separated by centrifugation. 1.0 mL phosphorus solution was extracted with a microporous syringe and filtered through a 0.22 m filtration membrane. The concentration of phosphorus was determined by UV–Visible spectrophotometer at wavelength of 700 nm. To determine the optimum conditions for phosphorus removal, the effects of dosage, temperature and pH were studied in detail. The phosphorus removal rate was calculated by Eq. (1):

$$R = \frac{(C_0 - C_e)}{C_0} \times 100\% \quad (1)$$

where R is the removal rate of phosphorus (%), C_0 (mg/L) is the initial concentration of phosphorus ions before adsorption, and C_e is the equilibrium concentration of phosphorus ions in the solution [24].

In addition, the adsorption capacity Q_e of phosphorus by Mg–Al/SF composite material was calculated by the following Eq. (2):

$$Q_e = \frac{(C_0 - C_e)}{M} \times V \quad (2)$$

where Q_e is the adsorption quantity of phosphorus (mg/g), M is the mass (g) of Mg–Al/SF composite material, and V is the volume (L) of solution [25–29].

Moreover, the corresponding adsorption kinetics and isothermal equilibrium were also investigated to explore the adsorption mechanism.

2.4 Regeneration Performance

Cyclic experiments were carried out to measure the cycling usability and stability of Mg–Al/SF adsorbent. The adsorbent that degraded 100 mL phosphorus solution in the previous time was collected, washed with clean water, and then dried. The adsorbent was added to 100 mL phosphorus solution again, and the R value was calculated under the same conditions. Continuous experiments were carried out to observe the reuse performance of Mg–Al/SF. Each experiment was repeated three times.

2.5 Apparatus

X-ray diffraction (XRD) analysis of the material was conducted on X-ray powder diffraction (Shimadzu XRD-6100) with a scanning rate of 5°/min. The morphologies of the as-prepared adsorbents were characterized by scanning electron

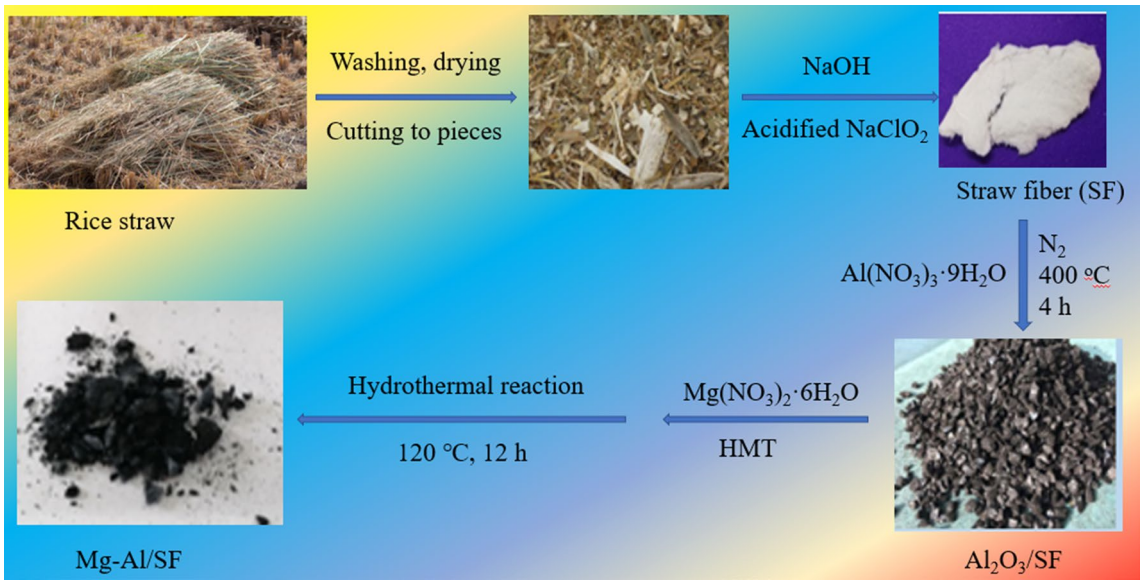

Scheme 1 The synthetic process of Mg–Al/SF

microscope (SEM Hitachi S-4800) with EDS function. X-ray photoelectron spectroscopy (XPS) was conducted on an Axis Ultra DLD (Kratos) spectrometer with Al mono Kα X-ray source (1486.71 eV photons). Specific surface area was studied by the Brunauer–Emmett–Teller (BET) method. FT-IR spectrum of the sample was obtained with an FT-IR spectrometer (AVATAR 360, Madison and Nicolet). A minimum of 32 scans was signal-averaged with a resolution of 2 cm^{-1} in the 4000–400 cm^{-1} ranges. The UV–Vis absorption spectrum was obtained in the range from 200 to 800 nm on an Agilent UV-1801 spectrophotometer.

3 Results and Discussion

3.1 Characterizations

SEM images of SF (A and B), Al_2O_3/SF (C and D) and Mg–Al/SF under different magnification are shown in the Fig. 1. As can be seen from Fig. 1A and B, the straw fibers were flat and over 40 μm in width. The microgrooves existed on the surface of the extracted straw fiber lead to the rough structure of the sample. The large width provided effective area for the construction of micro-nanomaterials, while the rough surface facilitated the adhesion of micro-nanomaterials. After coating with Al_2O_3, the pristine fiber structure was not been destroyed. The Al_2O_3 layer was dense without cracks, indicating the formation of high quality Al_2O_3 layer (Fig. 1C, D). After immersing in the $Mg(NO_3)_2$ solution for 12 h, Mg–Al/SF was obtained (Fig. 1E, F). Compared with Al_2O_3/SF, more uniform protrusions were formed on the surface of Mg–Al/SF, meanwhile, many wrinkles also appeared on the surface, which provided effective structural support and more active sites for Mg–Al/SF to improve its contact with phosphorus solution.

XRD patterns of SF, Al_2O_3/SF and Mg–Al/SF are shown in Fig. 2. It's clearly observed that an obvious absorption peak appeared at $2\theta = 23.8°$ in SF, which could be ascribed to carbon peak (JCPDS No. 50-0926). The high and sharp peak shape implied the high crystallinity of SF. After calcination, a relatively weak peak between 20° and 35° was corresponding to (012) reflection plane of Al_2O_3 (JCPDS No. 100173) in Al_2O_3/SF, indicating the formation of amorphous Al_2O_3 with low crystallinity. Meanwhile, the disappearance of carbon peak in Al_2O_3/SF indicated the thickness and density of Al_2O_3 layer. As shown in the curve of Mg–Al/SF, two peaks emerged at $2\theta = 44.89°$ and 66.98° represented the (200) and (220) reflection planes of MgO crystal (JCPDS No. 45-0946), further demonstrating the successful preparation of Mg–Al/SF.

The results of BET analysis of SF, Al_2O_3/SF and Mg–Al/SF are listed in Table 1. From Table 1, the Mg–Al/SF composite material had bigger specific surface area than the SF and Al_2O_3/SF. Moreover, the relative average pore diameter of Mg–Al/SF was larger than that of Al_2O_3/SF, which was positive to the effective adsorption of phosphorus by Mg–Al/SF. Therefore, Mg–Al/SF material could be employed as an efficient adsorbent for removal of phosphorus from wastewater due to the synergistic effect of the change between specific surface area and average pore size.

XPS was employed for qualitative analysis of elements in the material, as shown in the Fig. 3. As can be seen from Fig. 3A, the existing C, O, Mg and Al elements in Mg–Al/SF before and after adsorption suggested the successful preparation of Mg–Al/SF. And a new P element peak was observed after adsorption of phosphorus. Figure 3B presents the enlarged signal of P elements after adsorption, implying that the phosphorus in the simulative water was adsorbed on Mg–Al/SF. Figure 3C, D indicate the high-resolution XPS images of Al and Mg element. The peak strength of Al element did not change before and after adsorption, but the signal of Al 2p shifted to a higher energy level after adsorption, which might be ascribed to the electrostatic interaction between Al and PO_4^{3-}. In contrast, Mg 1 s signal was greatly weakened after adsorption, which may be due to the co-precipitation of Mg^{2+} with PO_4^{3-}. The chemical adsorption of PO_4^{3-} by Mg element reduced the content of Mg on the surface of Mg–Al/SF. In addition, FT-IR analysis was also carried out to investigate interaction between the sample with phosphates (Fig. 4). As shown, the adsorption band between 450-820 cm^{-1} is attributed to the pristine straw fiber. And the peak as 1597 cm^{-1} should be assigned to the water molecules arround the metal oxide [30]. It can also observed that the peak near 3400 cm^{-1} were represented the stretching vibration of O–H. After adsorption of phosphorus, two emerging peaks appear at 1030 and 1074 cm^{-1}, which are corresponded to the asymmetric stretching vibration of PO_4^{3-} [31]. The result is consistent with the XPS analysis above, indicating the successful adsorption process of Mg–Al/SF towards phosphorus.

3.2 Effects of pH and Temperature on Phosphorus Adsorption

The solution pH is a crucial factor in the adsorption process that may have influence on the surface structure and the ionization degree of the composite. To study the influence of pH, the adsorption temperature and the adsorption time was set at 45 °C and 2 h, the initial concentration of phosphorus solution was 100 mg/L and the dosage of Mg–Al/SF was 30 mg. As presented in the Fig. 5, the removal rate of phosphorus increased when the pH ranged from 3 to 6. However, as the pH value continued to increase to 10, the phosphorus removal rate showed a downward trend. The dissociation of the functional group at the active site under low pH condition has effect on the dissolution of the magnesium

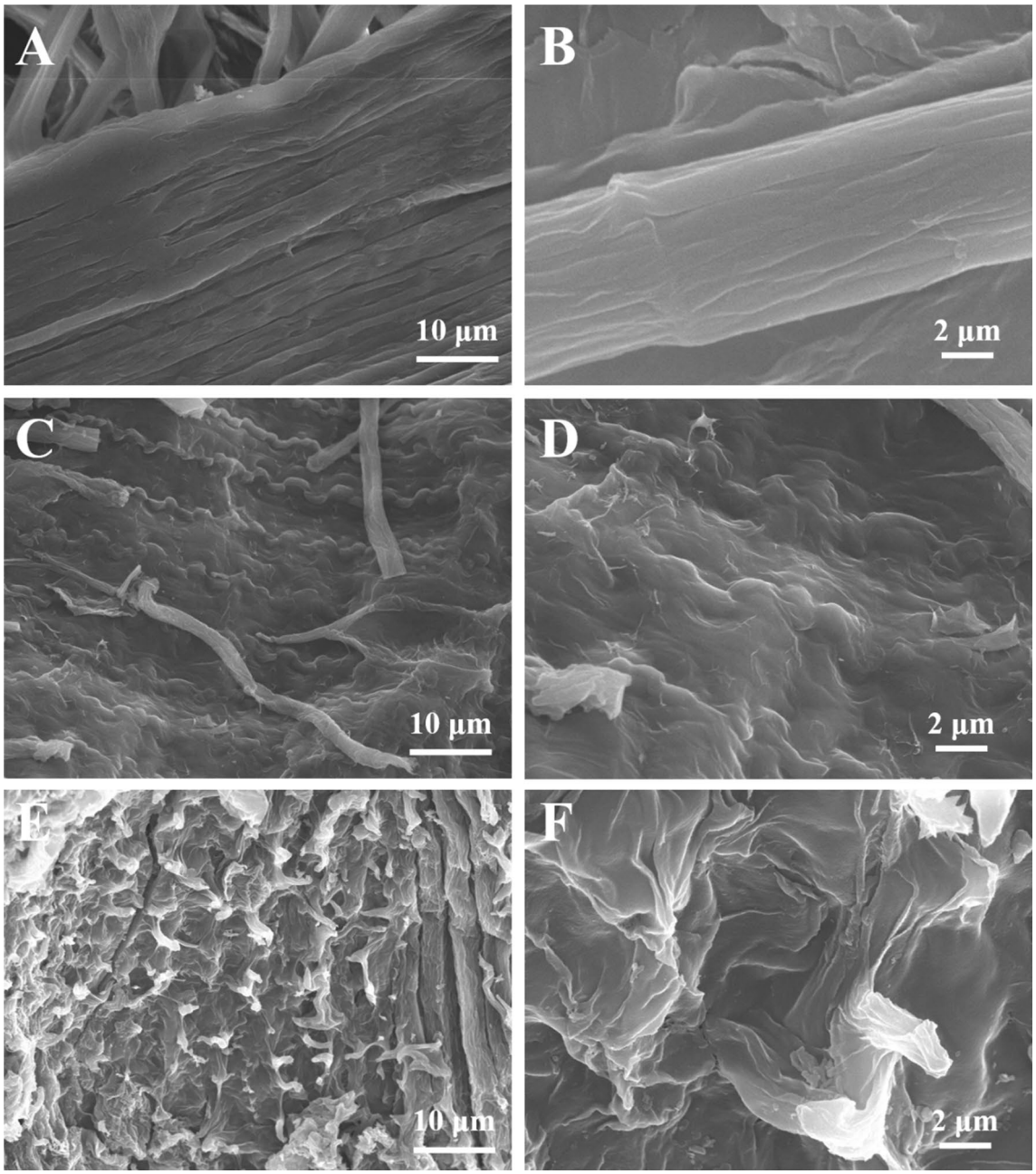

Fig. 1 SEM images of SF (**A** and **B**), Al_2O_3/SF (**C** and **D**) and Mg–Al/SF (**E** and **F**) at different magnification

aluminum oxide, resulting in the poor adsorption performance of Mg–Al/SF. Subsequently, with the increase of pH value, the content of $H_2PO_4^-$ gradually increased and the intensify of the electrostatic effect enhanced, resulting in the enhancement of adsorption capacity. Therefore, the optimal pH in this work was selected at 6.

The further study on temperature effect on phosphorus adsorption was carried out with different initial concentrations of phosphorus solution. The amount of Mg–Al/SF material was 30 mg with adsorption for 2 h and solution pH at 6.0. The results were shown in the Fig. 6. When the temperature increased from 25 to 45 °C, the removal rate of phosphorus increased from 87.32 to 96.08%. It implied that higher temperature was beneficial to the adsorption process, which further suggesting the endothermic process of phosphorus adsorption. Under high temperature, brownian motion of molecules was more violent, which is favor of enhancing the motion rate of molecules. In addition, the number of active sites for effective adsorption also increased during the adsorption process. It could be seen that the

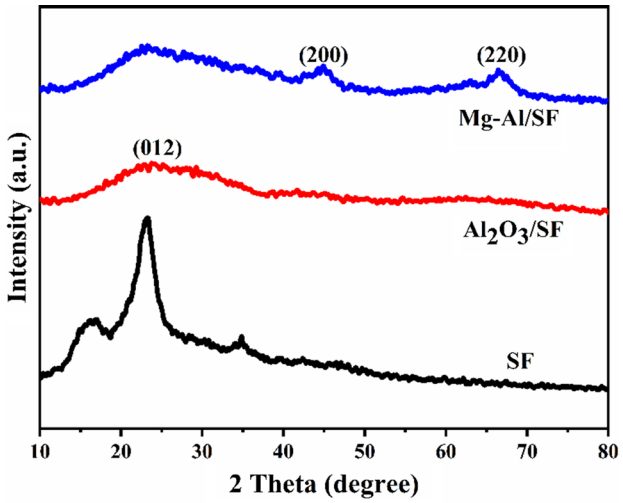

Fig. 2 XRD patterns of SF, Al_2O_3/SF and Mg–Al/SF

Table 1 The BET specific surface area and average pore of SF, Al_2O_3/SF and Mg–Al/SF materials

Samples	Specific surface area (m^2/g)	Average pore diameter (nm)
SF	27.11	3.89
Al_2O_3/SF	40.44	1.34
Mg–Al/SF	42.88	2.56

removal rate under 30 °C and 45 °C has not much difference, hence, the optimum temperature was set at 45 °C.

3.3 Effects of Adsorbent Dosage and Contact Time on Phosphorus Adsorption

The usage of adsorbent is also a nonnegligible factor in the adsorption process. Figure 7 shows the effect of different dosages of Mg–Al/SF on phosphorus removal rate with the initial concentration of phosphorus solution at 100 mg/L. Correspondingly, the adsorption temperature, pH and contact time were fixed at 45 °C, 6.0 and 2 h respectively. As can be seen from Fig. 7, the removal rate of phosphorus in the solution clearly enhanced as the dosage of Mg–Al/SF increased. The increase of the adsorbent dosage provided more adsorption active sites for the contact with adsorbate, thus improving the adsorption performance of phosphorus. In addition, when the adsorbent dosage was between 0 and 30 mg, the phosphorus removal rate increased rapidly, while the dosage was over 30 mg, the phosphorus removal rate reached its maximum value and remained stable. The high efficiency of phosphorus removal is mainly due to the larger specific surface area and more exposed adsorption sites of the composite. Considering of the general situation in the adsorption process, the optimal dosage of Mg–Al/SF was chosen 30 mg.

The results of different contact time are shown in the Fig. 8. It's clear that the removal rate of phosphorus improved when the contact time gradually increased. The removal rate of phosphorus was basically unchanged when the adsorption time exceeded 2 h. Taken together, the optimal adsorption time was set 2 h in this experiment.

3.4 Isotherm Study

The comparison between Langmuir model and Freundlich isothermal model are displayed in the Fig. 9. The initial concentration of phosphorus solution was ranged from 25 to 500 mg/L. Figure 9a, b presented the Langmuir isothermal adsorption and the fitting curve of Freundlich isothermal adsorption, respectively. The related parameters and correlation coefficients were all listed in Table 2.

The nonlinear fitting equations of the Langmuir and Freundlich isotherm models are expressed as follows, respectively [25]:

$$\frac{1}{q_e} = \frac{1}{q\max} + \frac{1}{K_L q\max C_e} \tag{3}$$

$$\ln q_e = \ln K_F + \frac{1}{n} \times \ln C_e \tag{4}$$

where q_e (mg/g) is the calculated equilibrium adsorption capacity, C_e (mg/L) is the equilibrium concentration of phosphorus. K_L and K_F are the Langmuir adsorption equilibrium constant and Freundlich adsorption equilibrium constant, respectively. 1/n is a measure of the exchange intensity or surface heterogeneity, with a value of 1/n smaller than 1.0 describing a favorable removal condition.

According to the calculated data in Table 2, the correlation coefficient of the Freundlich isothermal model was higher than that of the Langmuir isothermal model, implying that Freundlich isothermal model fitted better to describe the adsorption system. From Langmuir isothermal model, it can be seen that the maximum adsorption capacity q_{max} was 89.37 mg/g. The results demonstrated the outstanding adsorption performance of Mg–Al/SF. In addition, the value of 1/n in the Freundlich isothermal model was over 1, suggested the cooperative adsorption in the whole removal process of Mg–Al/SF towards phosphorus. The positive structural charge on the surface of Mg–Al/SF can form electrostatic attraction with negatively charged phosphate ions, which can be applied to capture phosphate in water through electrostatic interaction. Meanwhile, the anions and crystal water located in the interlaminar could break old bonds and form new bonds due to the weak chemical bond

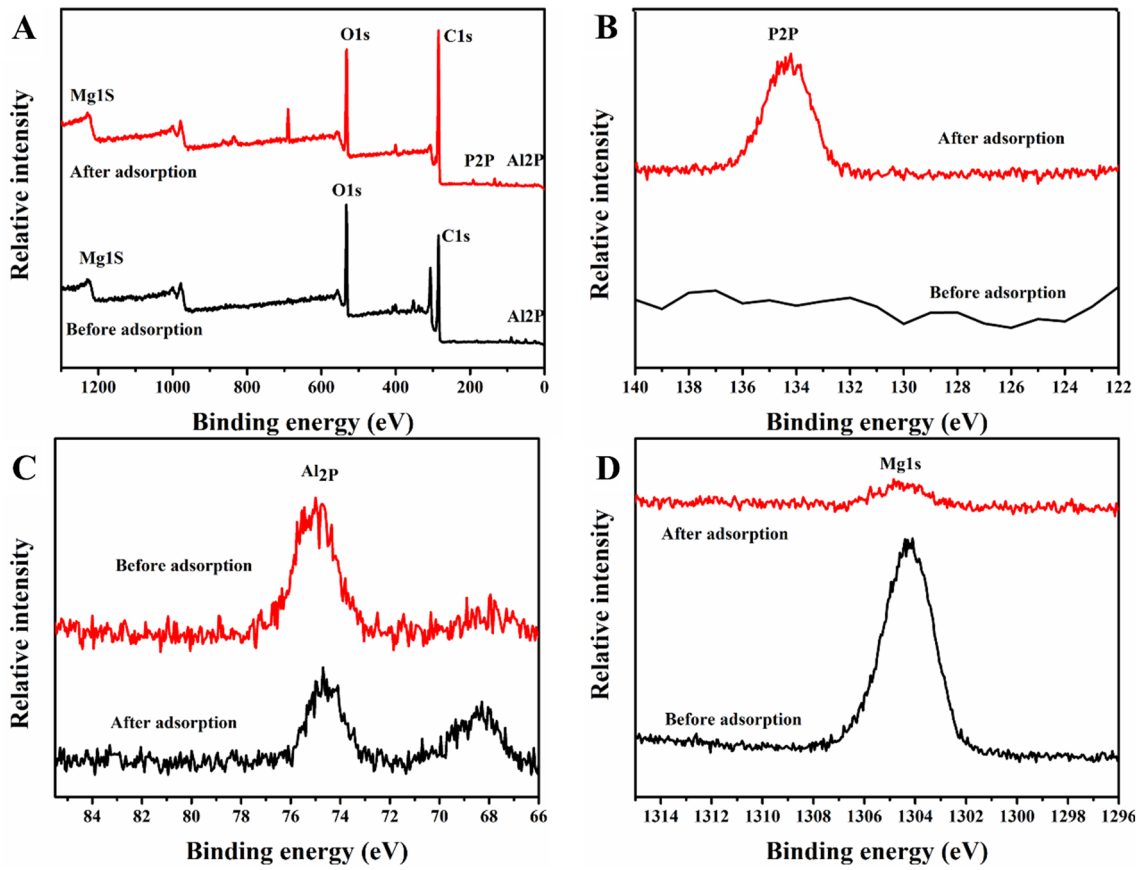

Fig. 3 X-ray photoelectron spectroscopy of Mg–Al/SF composites before and after adsorption

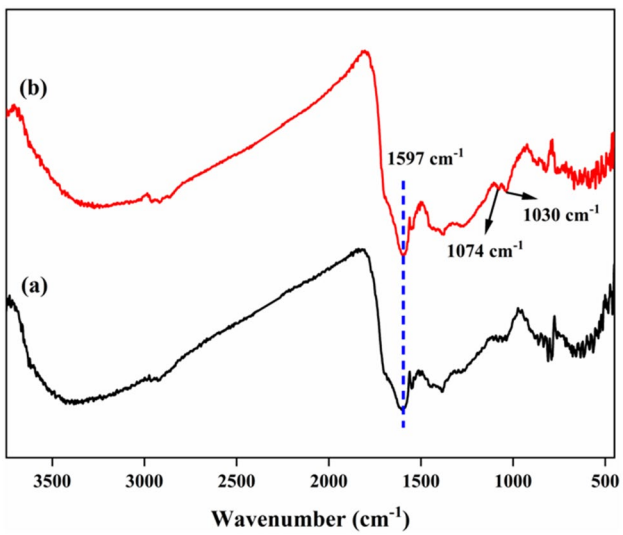

Fig. 4 FT-IR spectra of Mg–Al/SF before (**a**) and after (**b**) adsorption

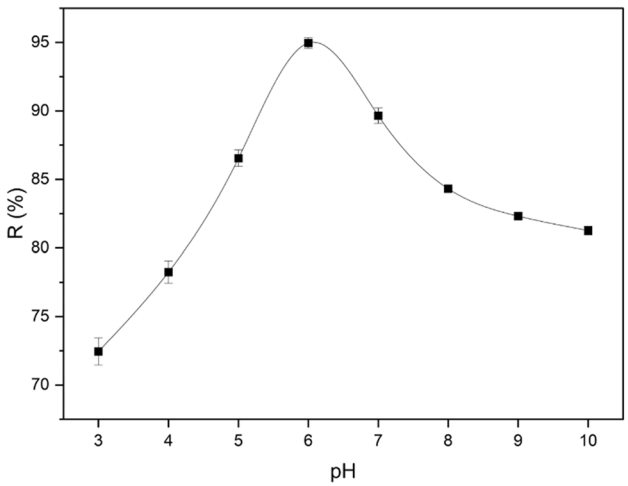

Fig. 5 Effect of pH on phosphorus adsorption

combinations between Mg–Al/SF and interlaminar anion or water molecular. Therefore, Mg–Al/SF can be used to remove phosphorus from the water.

3.5 Kinetics Study

To determine the key steps in the whole adsorption process, three kinetic models were used to analyze the adsorption process with different initial concentrations, namely,

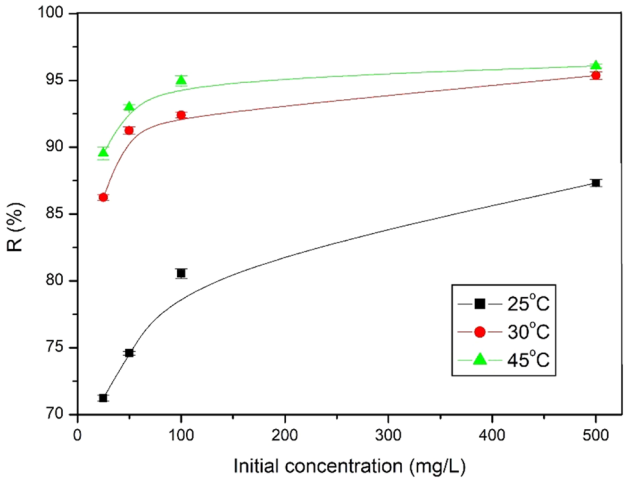

Fig. 6 Effect of different temperatures on removal rate

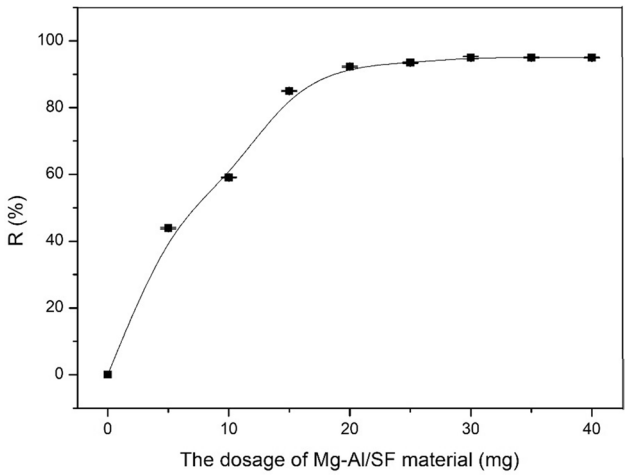

Fig. 7 Effect of different dosages of Mg–Al/SF on phosphorus removal rate

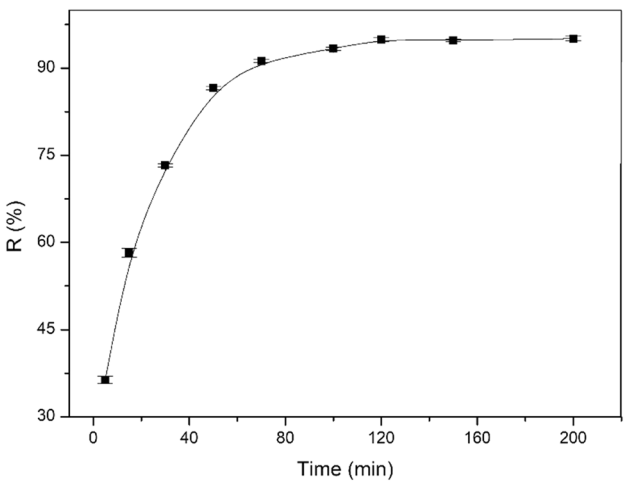

Fig. 8 Effect of contact time on phosphorus removal

pseudo-first-order model, pseudo-second-order model and the particle internal diffusion kinetic model. The adsorption kinetics was studied under the optimal adsorption conditions and the relevant results are shown in the Fig. 10. The mathematical expressions of the dynamic models are as follows Eqs. [5–7]:

$$\ln\left(q_e - q_t\right) = \ln q_e - k_1 t \tag{5}$$

$$\frac{t}{q_t} = \frac{1}{K_2 q_e^2} + \frac{t}{q_e} \tag{6}$$

$$q_t = K_p t^{\frac{1}{2}} + C \tag{7}$$

where q_e (mg/g) and q_t (mg/g) are the amounts of phosphorus on the adsorbent Mg–Al/SF at equilibrium and time t (min), respectively. K_1, K_2 and K_p shall be the adsorption rate constant for the pseudo-first-order model, pseudo-second-order model and internal diffusion kinetic model [32].

The fitting parameters of different kinetic models are listed in Table 3. According to the data in Table 3, the correlation coefficient of the pseudo-second-order model was the highest ($R^2 = 0.9997$), suggesting that the cooperative adsorption could describe the phosphorus adsorption well. Figure 10a, b shows the fitting curves of pseudo-first-order model and pseudo-second-order model, respectively. From the fitting linear curves in the Fig. 10, it could be deemed that the phosphorus adsorption process was the synergistic combination of surface adsorption and chemical adsorption. The surface adsorption could be ascribed to biomass fiber, while the chemical adsorption occurred mainly in the synergistic effect of alumina and magnesium oxide.

As for the particle internal diffusion kinetic model (Fig. 10c), the linear equation of particle internal diffusion fitting of Mg–Al/SF does not pass the origin of coordinates. And the fitting curve has an inflection point (Fig. 10d). Therefore, it can be offered that the adsorption process could be divided into the migration (external diffusion) process of adsorbent in the fluid boundary film around the adsorbent and the gentle adsorption process, and the diffusion process was the rate control step during the gentle adsorption process.

Several adsorbents reported in the previous investigations on phosphorus removal from wastewater are listed in Table 4. From the comparison on phosphorus adsorption quantity of Mg–Al/SF with other kinds of adsorbents, it can be revealed that the as-prepared adsorbent in this work exhibited competitive adsorption capacity. The adsorption capacity is far exceeding the reported phosphate adsorbents such as steel slag, sponge iron, sludge, etc. The adsorption quantity of Mg–Al/SF is almost the same with that of Al-MIL-101 adsorbent listed in Table 4, however, the rebinding

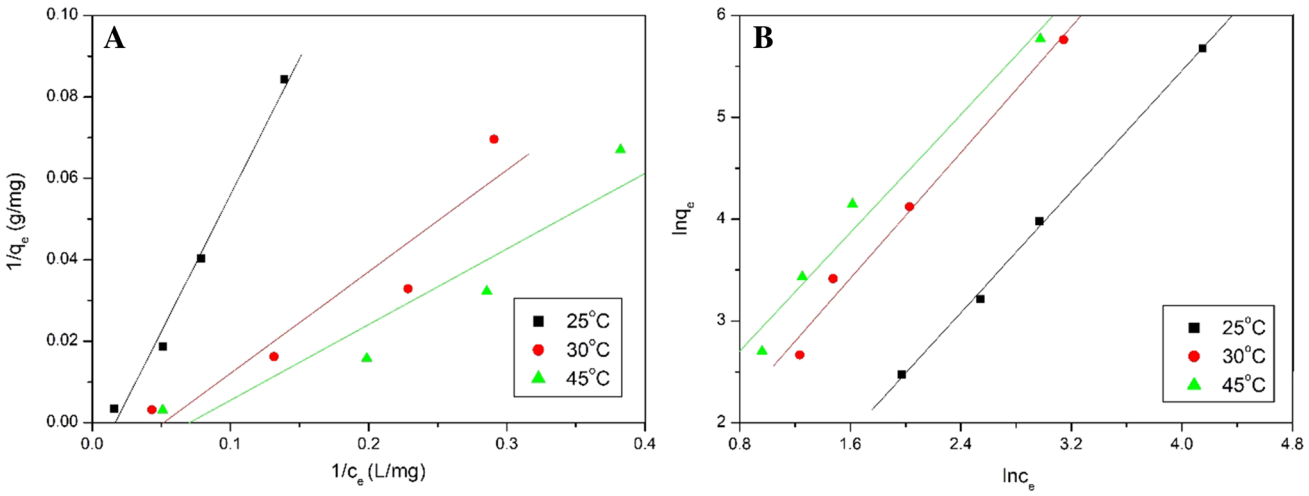

Fig. 9 Langmuir isotherm model (**a**) and Freundlich isotherm model (**b**)

Table 2 Adsorption isotherms parameters for phosphorus adsorption onto Mg–Al/SF material

Langmuir				Freundlich		
T(°C)	q_{max} (mg/g)	K_L (L/mg)	R^2	K_F	1/n	R^2
25	89.37	0.01667	0.9939	0.3710	0.6174	0.9991
30	77.64	0.05157	0.9448	1.3394	2.5764	0.9929
45	76.51	0.07035	0.9436	1.1328	4.6788	0.9966

time until equilibrium is much reduced from 12 h to 2 h. Moreover, the adsorption capacity of Mg–Al/SF is obviously enhanced when compared with other biomass-based material such as 40%Mg–Al biochar LDH. The data listed in Table 4 demonstrates that as-obtained Mg–Al/SF is an alternative adsorbent recycled from waste material to remove phosphorus from wastewater.

3.6 Adsorption Mechanism

The adsorption performance of adsorbent depends on its internal structure, crystal morphology and the size of active molecules. Mg–Al/SF has a hierarchical structure with large specific surface area, exposing more adsorption sites and facilitating the degradation of phosphorus in water. In addition, the synergistic effect between metal elements and biomass fiber plays an important role in phosphorus adsorption. Al_2O_3 as a unique amphoteric metal oxide, exhibits different properties under different conditions. When the isoelectric point of Mg–Al/SF is less than the pH value of phosphorus solution, the adsorbent surface is charged and alkaline, which can attract and adsorb phosphorus in water through electrostatic. Then the adsorbed phosphorus could be combined with magnesium oxide to form chemical adsorption. Furthermore, the three-phase synergistic effect among biomass carbon fiber, Al and Mg enhanced the specific surface area of the adsorbent as well as the adsorption site, thus improving the proton transfer rate and phosphorus adsorption rate. A possible pathway for the phosphorus adsorption using Mg–Al/SF composite was proposed and is shown in Fig. 11.

3.7 Thermodynamic study

The thermodynamics study of Mg–Al/SF composite towards phosphorus (100 mg/L) was carried out at different temperature (25 °C, 30 °C and 45 °C). The equilibrium constant K at different temperatures were calculated according to the following formula:

$$K = \frac{(C_o - C_e)V}{C_e M} = \frac{q_e}{C_e} \tag{8}$$

where C_0 and C_e are the initial concentration and adsorption equilibrium concentration (mg/L), respectively; V is the volume of the mixture (mL); M is the amount of the adsorbent (g).

According to the Van't Hoff equation, it can be expressed as follow:

$$\Delta G^o = -RT \ln K \tag{9}$$

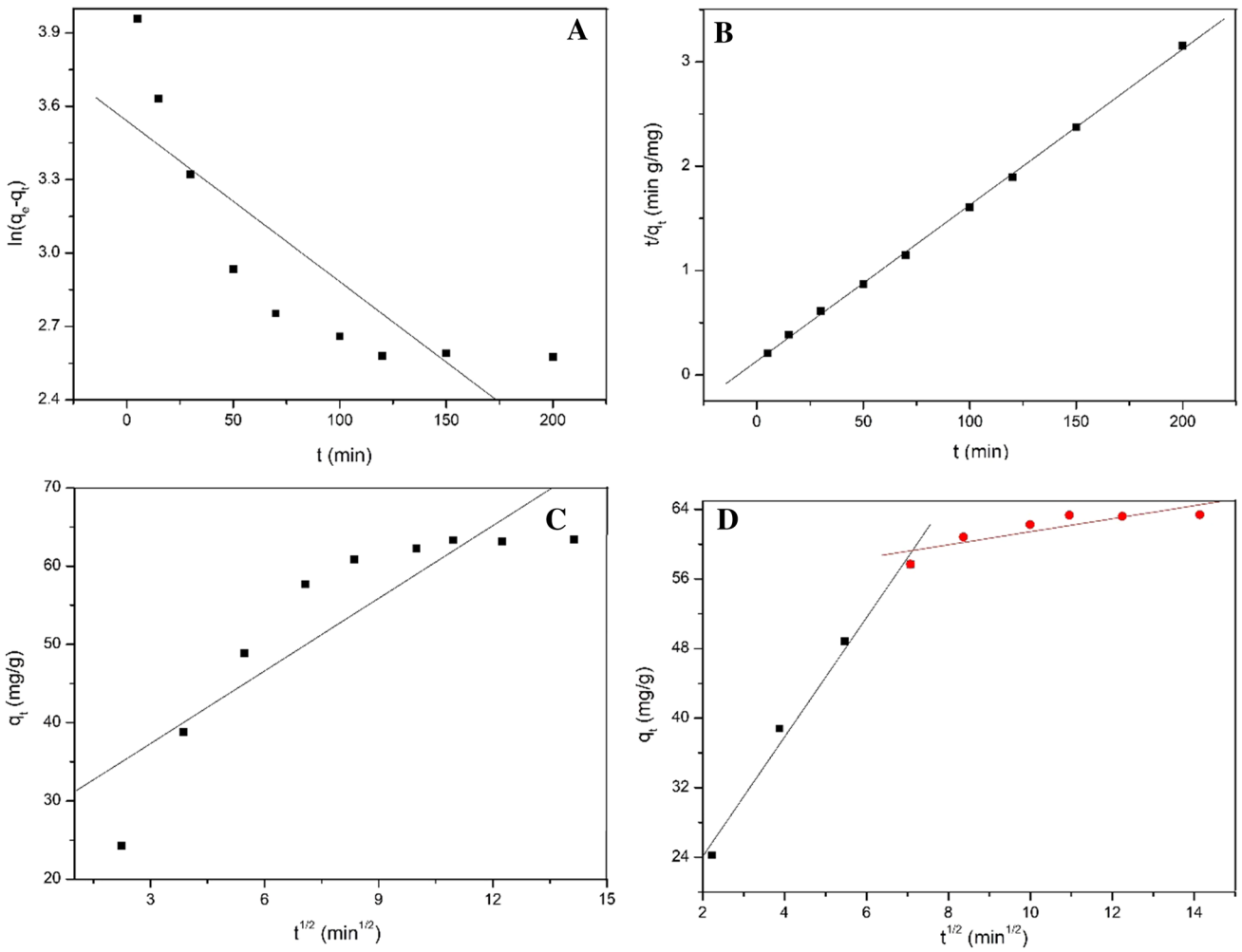

Fig. 10 The fitting curves of pseudo-first-order kinetic (**a**), pseudo-second-order kinetic (**b**) and internal diffusion kinetic (**c** and **d**) models

Table 3 The fitting parameters of kinetic model parameters

Pseudo-first order			Pseudo-second-order			Internal diffusion	
k_1 (L/min)	q_e (mg/g)	R^2	k_2 (g/(mg min))	q_e (mg/g)	R^2	k_p	R^2
0.00658	34.48	0.8399	0.01633	66.98	0.9997	3.09074	0.8854

Table 4 Previous studies on the adsorption of phosphorus with different adsorbents

Adsorbents	q_e (mg/g)	References
Steel slag filler	3.1	[33]
IDS-silica adsorbent	0.23	[18]
Sponge iron	3.25	[19]
Slag ceramsite filler	10.5	[31]
Alum-based sludge	47.62	[34]
Al-MIL-101	90	[22]
Zn-Al LDH	53	[35]
40%Mg–Al biochar LDH	32.1	[6]
Mg–Al/SF	89.37	This work

$$\Delta G^o = \Delta H^o - T\Delta S^o \tag{10}$$

$$\ln K_c = -\frac{\Delta H^o}{RT} + \frac{\Delta S^o}{R} \tag{11}$$

where ΔH^o(KJ/mol) and ΔS^o(J/(mol·K)) are enthalpy and entropy change, respectively. ΔG^o(KJ/mol) was the adsorption free energy. R is the gas constant (8.314 J/(K·mol)). T is the absolute temperature (K).

It could be calculated that $\Delta H^o = 49.63$ kJ/mol and $\Delta S^o = 177.75$ J/(mol·K). The calculation results from thermodynamic parameters showed that both ΔH^o and ΔS^o were positive. ΔG^o was negative, which indicated that the adsorption

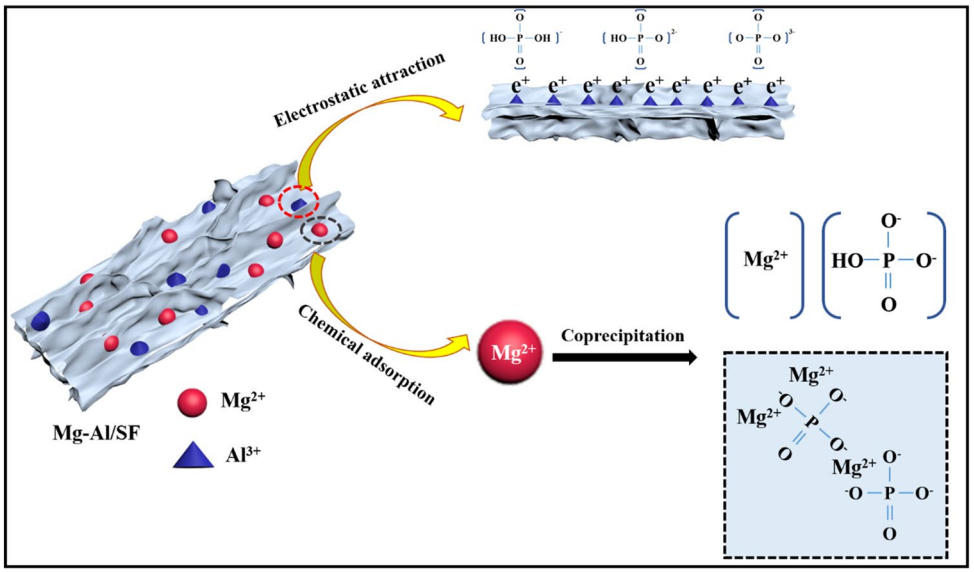

Fig. 11 A possible pathway for the phosphorus adsorption using Mg–Al/SF composite

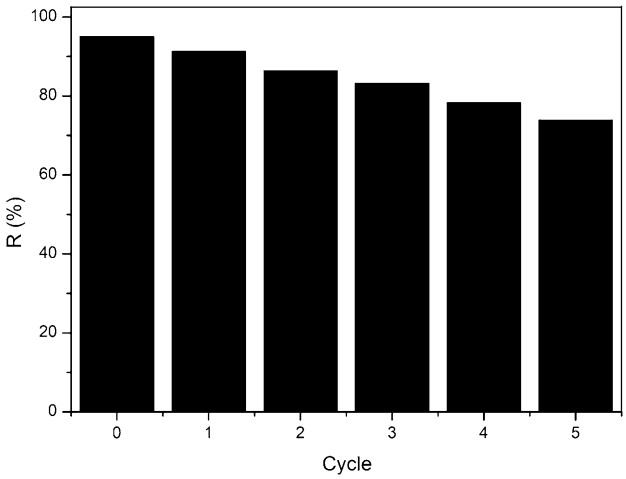

Fig. 12 Recycling performance of Mg–Al/SF composites

of phosphorus by Mg–Al/SF was spontaneous. The results implied that the adsorption of phosphorus was an endothermic reaction and high temperature is favorable for adsorption, which is consistent with the experimental results above.

3.8 Regeneration Performance of Mg–Al/SF

To explore the regeneration capacity of the material, the phosphorus adsorption–desorption experiment was performed, and the results are shown in the Fig. 12. The results showed that the phosphorus removal rate of the material decreased to a certain extent with the increase of recycling times. After five times of recycling, the phosphorus removal rate of the material dropped to 72%. The reason could be explained by the occupation of part of active sites and hydrolyzation of magnesium aluminum oxide on the surface. Despite this, the prepared adsorbent still possessed good reuse performance and stability.

3.9 Practical Application

To investigate the practical application effectiveness of Mg–Al/SF material, actual domestic sewage was applied to carry out static adsorption test. By comparing with the adsorption performance of commercial activated carbon, the removal of total phosphorus in actual domestic sewage (Total phosphorus, TP, 0.8–1.1 mg/L) are investigated. The adsorption materials, Mg–Al/SF and commercial activated carbon (CCA), were repeatedly washed with deionized water, dried and stored for standby. The static adsorption experiments of phosphorus in domestic sewage were carried out, and removal of total phosphorus (TP) were measured. The specific steps are as follows: The impurities were removed from the domestic sewage samples. Mg–Al/SF or CCA was added into domestic sewage sample solution (100 mL). The adsorption system was conducted at room temperature. The removal of total phosphorus was determined at different time; and the results are shown in the Fig. 13. As can be seen from Fig. 13, the prepared Mg–Al composite oxide/rice straw carbon fiber composite (Mg–Al/SF) has excellent TP adsorption performance, and the adsorption performance is significantly higher than that of the commercial activated carbon.

To explore the practical recycling performance of the Mg–Al/SF and CCA material, the phosphorus adsorption–desorption cycle experiment was carried out, and the results are shown in the Fig. 14. When the adsorption time was 200 min, the average TP removal rate of Mg–Al/SF is much higher than that of commercial activated carbon (CCA); and has excellent recycling performance and stability. Therefore,

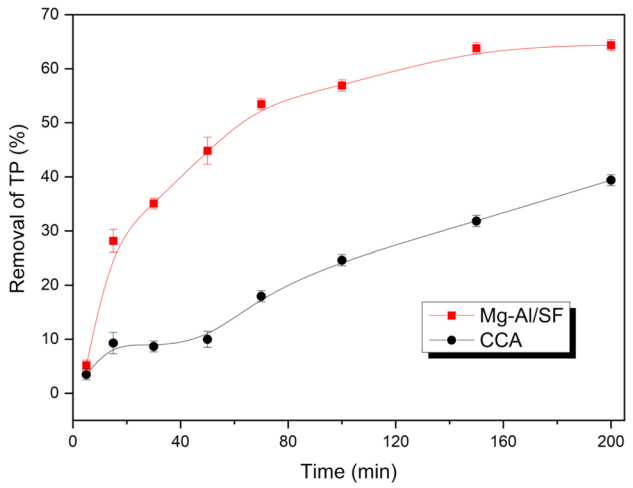

Fig. 13 Comparison of TP removal: Mg–Al/SF and CCA materials

the Mg–Al/SF material in this work provides a useful idea for the removal of total phosphorus from wastewater in the future.

4 Conclusions

In this work, a novel biomass-based adsorbent derived from agricultural waste was successfully synthesized via hydrothermal method incorporated with in situ growth method. Abandoned straw was selected as precursor for the extraction of biomass carbon fibers. After alkali treatment and simple decolorization, biomass carbon fibers were used as substrate for the constructing of magnesium–aluminum composite oxide layer to prepare Mg–Al/SF adsorbent. Adsorption experimental results showed that the synthesized Mg–Al/SF had high adsorption capacity and good reusability in the removal of phosphorus. The maximum adsorption capacity could reach 89.37 mg/g under the optimum adsorption condition. The Freundlich isothermal model fitted better to the experimental data and the adsorption process conformed to the pseudo-second-order model. In addition, the removal rate of phosphorus remained above 72% after 5 cycles. The adsorption mechanism can be explained by the combination of physical adsorption and chemical adsorption. The synergistic effect of biomass carbon, alumina and magnesium oxide made Mg–Al/SF a promising adsorbent for phosphorus removal. The prepared Mg–Al/SF material has the bigger removal of TP than the commercial activated carbon. It's expected that materials produced from natural waste can be economical adsorbents and the proposed strategy could be applied in other area for wastewater treatment.

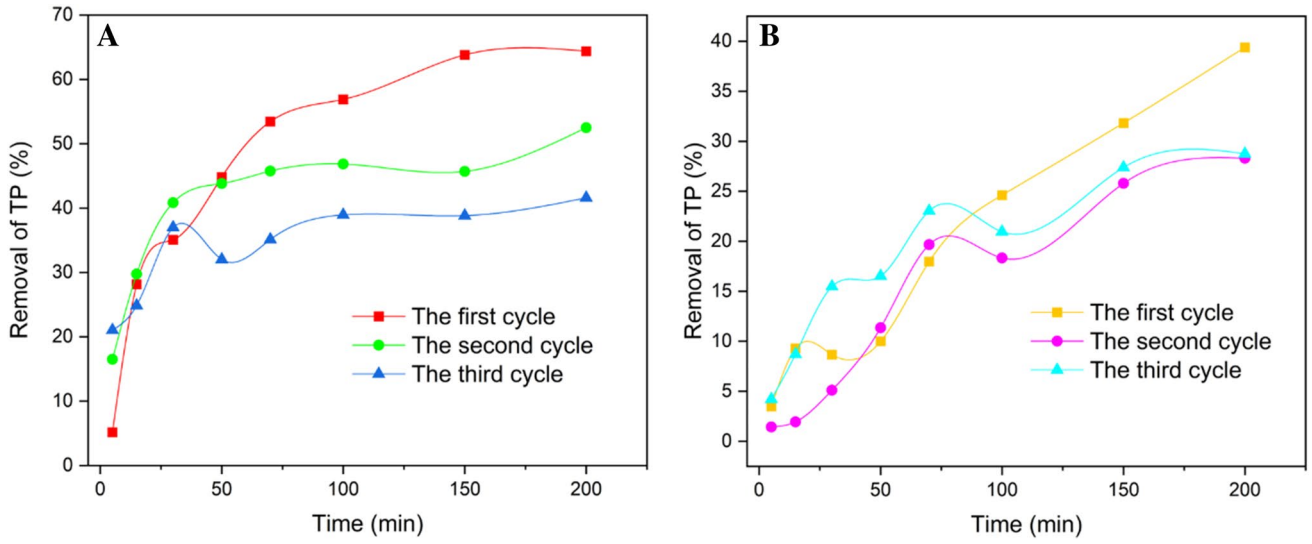

Fig. 14 Comparison of recycling performance: Mg–Al/SF (**a**) and CCA (**b**) materials

Acknowledgements This work was supported by the National Nature Science Foundation of China (21878132).

References

1. J. Li, F. He, X. Shen, D. Hu, Q. Huang, Bioresour. Technol. **315**, (2020)
2. T. Zhang, D. Yuan, Q. Guo, F. Qiu, D. Yang, Z. Ou, Food Bioprod. Process. **114**, 154–162 (2019)
3. J. Yuan, Y. Zhu, J. Wang, L. Gan, M. He, T. Zhang, P. Li, F. Qiu, Food Bioprod. Process. **126**, 293–304 (2021)
4. J. Wang, W. Qian, Y. He, Y. Xiong, P. Song, R. Wang, Waste Manage. **65**, 11–21 (2017)
5. L. Zhang, X. Peng, L. Zhong, W. Chua, Z. Xiang, R. Sun, Cur. Med. Chem. **26**, 2456 (2019)
6. S. Wan, S. Wang, Y. Li, B. Gao, J. Ind. Eng. Chem. **47**, 246–253 (2017)
7. Z. Chen, T. Huang, Y. Feng, W. Hu, F. Mao, C. Zhang, Y. Liu, Z. Fu, B. Chem, Soc. Jpn. **92**, 1824–1833 (2019)
8. S. Foong, R. Liew, Y. Yang, Y. Cheng, P. Yek, W. Maharib, X. Lee, C. Han, D. Vo, Q. Le, M. Aghbashlo, M. Tabatabaei, C. Sonne, W. Peng, S. La, Chem. Eng. J. **389**, (2020)
9. B. Sharma, B. Vaish, U. Singh, P. Singh, R. Singh, Int. J. Environ. Res. **13**, 409–429 (2019)
10. G. Oscar, M. Claudio, S. Bruna, I. Silvana, K. Guilherme, M. Andrés, C. Pio, O. Marcelo, G. Alice, L. Neftali, Cellulose **27**, 113–126 (2020)
11. H. Liu, P. Li, T. Zhang, Y. Zhu, F. Qiu, Food Bioprod. Process. **119**, 257–267 (2020)
12. Z. Jing, J. Ding, T. Zhang, D. Yang, F. Qiu, Q. Chen, J. Xu, Food Bioprod. Process. **115**, 134–142 (2019)
13. H. Liu, P. Li, F. Qiu, T. Zhang, J. Xu, Food Bioprod. Process. **123**, 177–187 (2020)
14. G. Morse, S. Brett, J. Guy, J. Lester, Sci. Total Envir. **212**, 69–81 (1998)
15. S. Aslan, I. Kapdan, Ecol. Eng. **28**, 64–70 (2006)
16. Z. Qin, A. Shober, K. Scheckel, C. Penn, K. Turner, J. Environ. Qual. **47**, 1232–1241 (2018)
17. H. Zou, Y. Wang, Bioresource Technol. **211**, 87–92 (2016)
18. I. Ashraf, C. Li, T. Wang, R. Li, B. Chen, Anal. Method. **12**, 466–470 (2020)
19. R. Xue, J. Xu, L. Gu, L. Pan, Q. He, Water Air Soil Poll. **229**, 161 (2018)
20. J. Torit, D. Phihusut, Environ. Sci. Pollut. Res. **26**, 34101–34109 (2019)
21. L. Qiu, M. Zhang, X. Yu, P. Zheng, Environ. Sci. Pollut. Res. **25**, 1543–1550 (2018)
22. S. Li, F. Jiang, M. Liu, Y. Wang, S. Wang, X. Yang, J. Colloid Interface Sci. **560**, 321–329 (2019)
23. L. Rugnini, G. Costa, R. Congestri, S. Antonaroli, L. Sanita di Toppi, L. Bruno, Plant Physiol. Biochem. **125**, 45–51 (2018)
24. G. Wu, W. Xing, J. Han, P. Li, Fresen. Environ. Bull. **29**, 445–453 (2020)
25. Y. Zhu, J. Rong, T. Zhang, J. Xu, Y. Dai, F. Qiu, Appl. Nanosci. **8**, 1139–1148 (2018)
26. Y. Zhu, F. Qiu, J. Rong, T. Zhang, K. Mao, D. Yang, Colloid. Surface B **191**, (2020)
27. Y. Zhu, J. Rong, K. Mao, D. Yang, T. Zhang, F. Qiu, J. Pan, Appl. Organomet. Chem. **34**, (2020)
28. H. Yu, T. Zhang, Z. Jing, J. Xu, F. Qiu, D. Yang, L. Yu, Chem. Eng. Sci. **205**, 278–286 (2019)
29. Y. Wang, J. Xu, X. Xu, D. Yang, X. Zheng, J. Pan, T. Zhang, F. Qiu, C. Li, Appl. Organomet. Chem. **32**, (2018)
30. F. Hu, M. Wang, X. Peng, F. Qiu, T. Zhang, H. Dai, Z. Liu, Z. Cao, Colloid Surface A. **555**, 314–323 (2018)
31. X. Liu, S. Yang, S. Liu, Y. Yang, Process Saf. Environ. **148**, 858–866 (2021)
32. Y. Wang, J. Xu, D. Yang, T. Zhang, F. Qiu, J. Pan, Appl. Organomet. Chem. **32**, (2018)
33. I. Blancoa, P. Molleb, L. Mierac, G. Ansola, Water Res. **89**, 355–365 (2016)
34. K. Krishna, A. Aryal, T. Jansen, J. Environ. Manage. **180**, 17–23 (2016)
35. H. Hatami, A. Fotovat, A. Halajnia, Appl. Clay Sci. **152**, 333–341 (2018)